

GRB-selected galaxies through cosmic time

T. Krühler*

European Southern Observatory, Alonso de Córdova 3107, Vitacura, Casilla 19001, Santiago 19, Chile

Received 2015 Feb 25, accepted 2015 Mar 14

Published online 2015 Jun 22

Key words gamma rays: bursts – galaxies: abundances – galaxies: high-redshift – galaxies: star formation

To use the luminous gamma-ray bursts and their afterglows as messengers from the early Universe has been advocated ever since the discovery of the cosmological nature of the GRB phenomenon in the late nineties. It took, however, until the advent of *Swift* to detect high-redshift GRBs in significant numbers, and to provide the localization capabilities to enable statistical samples of GRBs free of selection biases and complete in redshift. I will present and discuss some of the recent progress in the field, with an emphasis on new results derived from sample studies and their implications for the nature of GRBs and their host galaxies. I will particularly focus on observations made with the seven-channel imager GROND and X-shooter, an optical/NIR echelle spectrograph mounted at the Very Large Telescope since 2009.

© 2015 WILEY-VCH Verlag GmbH & Co. KGaA, Weinheim

1 Introduction

Long-duration gamma-ray bursts (GRBs) mark the rare explosive endpoint of the evolution of some massive stars (Hjorth et al. 2003; Pian et al. 2006), most likely fast-rotating Wolf-Rayet stars. GRBs are thus tightly associated to star-formation. The extreme energies and highly-relativistic jets that are emitted during the GRB and the multi-wavelength afterglow that follows it make them the most luminous objects in the Universe (see, e.g., Kumar & Zhang 2014, for a recent review). GRBs are hence cosmological objects observable out to the greatest distances. To date, the most distant spectroscopically-confirmed GRBs are GRB 080913 at $z = 6.7$ (Greiner et al. 2009) and GRB 090423 at $z = 8.2$ (Tanvir et al. 2009).

These two properties, extreme luminosities and association with star formation, make GRBs unique probes of galaxies. In detail, GRBs provide means of studying star-forming galaxies at the highest redshifts (e.g., Tanvir et al. 2012), faintest luminosities (e.g., Vreeswijk et al. 2001) as well as the global star-formation rate (SFR) density up to the epoch of re-ionization (e.g., Kistler et al. 2009; Robertson & Ellis 2012). In particular, the information that is obtained through afterglow spectroscopy provides insights of unprecedented detail into the chemical composition of high-redshift galaxies (e.g., Fynbo et al. 2006; Prochaska et al. 2009).

The *Swift* satellite (Gehrels et al. 2004) with its suite of instruments sensitive from hard X-rays (BAT) over soft X-rays (XRT) to the ultra-violet/optical (UVOT) energy range has enabled for the first time to study GRB and their afterglows in larger numbers and a well-controlled selection. With around 100 GRBs detected per year and routinely lo-

calized to $2''$, it has provided the seminal step to facilitate the use of GRBs as probes of the early Universe.

The GRB and its afterglow are transient events. Typical timescales for the prompt γ -ray emission are few to several hundred seconds, while the longer wavelength X-ray or optical/NIR afterglow is observable for a couple of hours or days. The afterglow, however, fades fast with $F_\nu \propto t^{-0.5\dots 1}$, and detailed high-resolution studies that are feasible a couple of minutes after the GRB trigger with a modest investment of observing time become impossible for even the largest telescopes very soon after.

The recent years have seen the advent of a number of instruments dedicated to the follow-up of optical/NIR afterglows. Specialized on a very-fast response to GRB triggers, with excellent sensitivity and broad wavelength coverage, these instruments exploit the GRB's unique possibilities much better than conventional instrumentation.

This contribution focuses on new results from those instruments, in particular from the optical/NIR multi-channel imager GROND (Greiner et al. 2008) mounted at the 2.2 m MPG/ESO telescope on LaSilla, as well as from the broad-band, medium-resolution spectrograph X-shooter at the VLT.

2 The nature of dark GRBs

A fundamental problem that has plagued demographic studies of GRBs for a long time was the presence of so-called optically-dark GRBs. These are the 30–50 % of all GRBs where an optical afterglow is absent or significantly underluminous compared to an extrapolation from X-ray observations.

Before *Swift*, an optical afterglow and its accurate localization was usually required to obtain a GRB redshift. Dark

* Corresponding author: t.kruehler@gmail.com

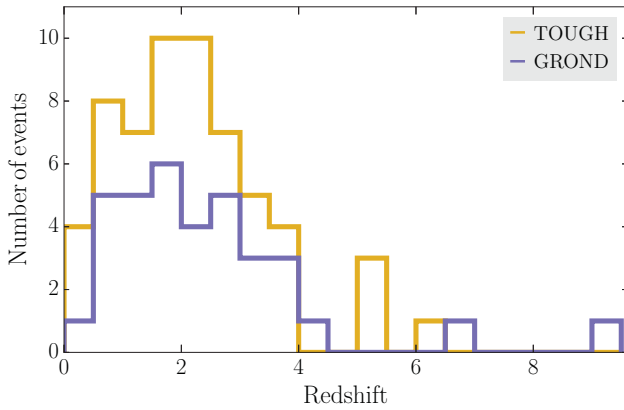


Fig. 1 Redshift distribution for GRBs from the GROND and TOUGH samples.

GRBs thus implied unknown systematic biases in GRB or host properties and thus their sample distributions. Because of a lack of deep follow-up in the optical/NIR, it was further unclear for a long time whether these dark afterglows were intrinsically faint, extinguished by dust (i.e., a high visual attenuation A_V), or absorbed by the $\text{Ly}\alpha$ and Ly-limit breaks redshifted into the observing band (i.e., a redshift above $z \sim 4$). Previous redshift-dependent GRB and GRB host samples were thus notoriously incomplete and were lacking a significant and fundamental contribution of high- z and/or high- A_V afterglows. Only the accurate X-ray positions from *Swift*/XRT allowed researchers to address this problem.

An accurate position, coupled with the increased sensitivity and NIR response that instruments like GROND provide, yielded for the first time redshift-complete GRB samples, i.e. nearly all satellite-detected GRBs had a measured afterglow and redshift. For example, Greiner et al. (2011) used GROND to detect 90% of all GRB optical/NIR afterglows whenever the observations started within less than four hours after the trigger. GROND not only provides the sensitivity to detect and study the very-early afterglow, but also a photometric redshift estimate at $z > 3$, or, together with UVOT at $z > 1.0$ (Krühler et al. 2011b). This proves crucial in cases where spectroscopic observations do not reveal emission/absorption lines, or are unfeasible, for example when the optical/NIR afterglow is too faint for spectroscopy.

2.1 An unbiased GRB redshift distribution

A first direct result of these samples were accurate GRB redshift distributions. Figure 1, for example, shows those of two highly complete and independent GRB samples: GRBs followed-up early after the trigger with GROND (Greiner et al. 2011) and GRBs from the TOUGH survey (Hjorth et al. 2012 and Sect. 3.1), with redshift completenesses of 92% and 86%, respectively.

These data constrain the fraction of *Swift*-GRBs above $z > 5$ to around $5 \pm 3\%$ in total and $\sim 25\%$ of all dark

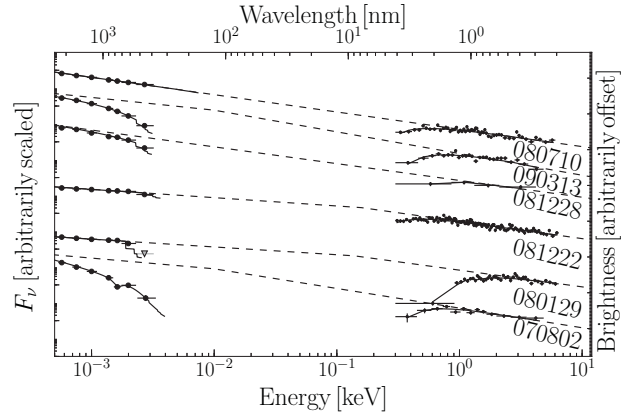


Fig. 2 Example SEDs from GROND (low-energy data) and *Swift*/XRT (high-energy data). The data are fitted with a synchrotron model for the underlying GRB afterglow emission, shown in dashed lines, modified by absorption of dust and gas in the GRB host galaxy, shown with black solid lines (adapted from Greiner et al. 2011).

bursts. Similar results are obtained by using the robotic P60 and observations within 1 hour after the trigger (Cenko et al. 2009), and deep late Keck follow-up to assess the degeneracy between high- z versus high A_V (Perley et al. 2009).

2.2 GRB afterglows as probes of dust

The majority of dark afterglows ($\sim 75\%$) is under-luminous because of dust extinction along the sight line to the GRB. Already one of the first afterglows observed by GROND, GRB 070802, revealed a significant amount of dust with $A_V \sim 1$ mag in its host galaxy through analysis of the afterglow's broad-band spectral energy distribution (Krühler et al. 2008). This provided the first and clearest detections of the 2175 \AA feature at high redshift, providing strong evidence for a carbon-rich environment and that Milky Way or Large Magellanic Cloud like dust was already formed in substantial amounts in a galaxy at $z = 2.45$.

Figure 2 shows as example the broad-band SED analysis of a small sample of GROND-observed GRBs together with XRT data. By fitting the g' to K_S band photometry and X-ray observations, the afterglow emission is constrained over 4 decades in energy, and features of the gas (soft X-rays) and dust absorption (rest-frame optical and UV) can be measured with a much higher accuracy than with other extra-galactic probes.

Similar analysis has now established the distribution of visual attenuations for statistically significant and representative samples of GRBs (Covino et al. 2013; Greiner et al. 2011): About 50–60% of all afterglows are essentially unabsorbed with $A_V < 0.2$ mag, another 20–30% are in the range of $0.2 \text{ mag} < A_V < 1$ mag, and 10–20% have a sight-line with $A_V > 1$ mag.

2.3 The hosts of dark GRBs

To assess the effect of the absence of well-localized dark GRBs in previous studies, we started to search systematically for these host galaxies (Krühler et al. 2011a, 2012). Again, the XRT observations and GROND data proved crucial in this search, because only accurate position allowed us to identify and study those hosts in detail.

After an initial photometric identification of GRB-associated galaxies, we measured their redshift from nebular emission line with spectroscopy. With a measured host redshift, the darkness of the GRB can then be unambiguously related to dust along its sight line.

Subsequently, we obtained multi-band imagery to model the galaxy SED with stellar population synthesis models in a standard fashion. This procedure yields parameters like galaxy luminosity and stellar mass and provide an extensive picture of dark GRB hosts. Their properties can then be compared against GRBs with bright optical afterglows (Krühler et al. 2011a).

Figure 3 shows such a comparison for GRB hosts selected at $z \sim 1.5$, where the stellar mass and B -band luminosity is used to investigate differences between the two samples. The hosts of the dustiest afterglows are diverse in their properties, but on average redder ($\langle (R - K)_{AB} \rangle \sim 1.6$ mag), more luminous ($\langle L \rangle \sim 0.9 L^*$), and massive ($\langle \log M_*/M_\odot \rangle \sim 9.8$) than the hosts of optically-bright events. Hence, optically-dark GRBs select a different galaxy population, suggesting that previous host samples missed most of the massive and metal-rich members because usually dark GRBs were not localized accurately enough.

This indicated that the properties of GRB hosts are diverse, and complex selection biases are present in older samples: not only are the very faintest GRB hosts missing because of the inherent sensitivity limits, but also some of the brightest, most luminous, and chemically-evolved ones. It thus became clear for the first time that dusty, metal-rich galaxies with a high stellar mass are able to host GRBs in significant numbers, a result similar to that obtained by Rossi et al. (2012) and Perley et al. (2013).

3 GRB-selected galaxies in emission

The GRB explosion represents a very rare endpoint of stellar evolution, and could thus be subject to environmental factors enhancing or quenching the GRB rate with respect to star-formation. The exact relation between SFR and GRB rate is thus controversial. For instance, a low metallicity of the progenitor star has often been discussed as being a fundamental condition for GRB formation. A physical understanding of GRBs and the galactic environments in which they form is thus necessary to put observations of high- z GRBs into a cosmological context. Arguably, one of the key pieces to the puzzle of understanding GRB progenitors and their role in probing distant star-formation lies in the nature of their host galaxies.

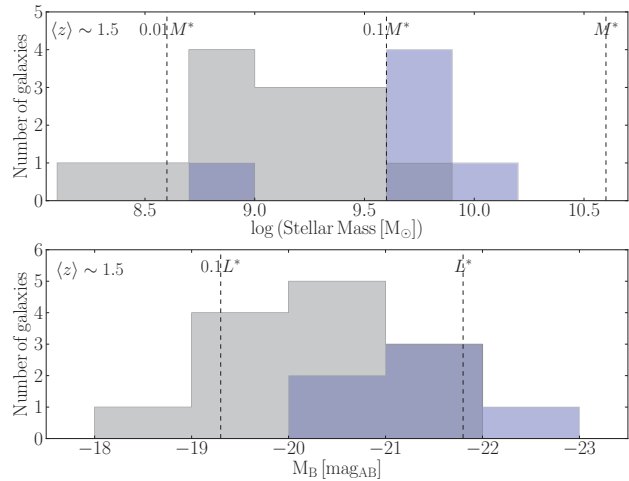


Fig. 3 Comparison between the hosts of optically-bright and optically-dark GRBs at $z \sim 1.5$. The former are plotted in grey, the latter in light-blue. The lower panel shows absolute B -band luminosity, the upper panel stellar mass. The hosts of dark GRBs are more luminous and more massive compared to the ones of optically-bright events at a similar redshift. Taken from Krühler et al. (2011a).

3.1 The TOUGH survey

The Optically Unbiased GRB Host survey, or short TOUGH (Hjorth et al. 2012), was the first survey of GRB-selected galaxies to provide a well-defined and homogeneous GRB subsample that is independent on physical or observational biases. In total, TOUGH contains 69 individual GRBs. To search for their hosts, the GRB fields were observed to deep limits with the VLT in the R and K bands. This provides a very high detection rate (80% of all GRBs have detected hosts). Because of additional extensive spectroscopic follow-up efforts (Jakobsson et al. 2012; Krühler et al. 2012), TOUGH has now achieved an exquisite redshift completeness (85% of all GRBs have redshifts), and has a median redshift of $z_{\text{med}} = 2.06 \pm 0.18$.

The first primary results from the TOUGH survey was the detection of a significant number of $z > 1$ GRB hosts (see Figure 4). These include 17 systems at $z > 2$, covering a wide range of luminosities from $0.1 L^*$ to around L^* . GRB-hosting galaxies from TOUGH tend to be blue, but somewhat redder than those found previously (Fig. 4).

TOUGH confirmed for the first time with a homogeneously-selected sample that galaxies that hosted GRBs with detected optical/NIR afterglow are significantly less luminous and bluer than those without (Sect. 2.3). In addition to these results, TOUGH also provided a sensitive survey for $\text{Ly}\alpha$ emitters among high- z GRB hosts, as well as follow-up in the radio wavelength range. For further details, I refer to Milvang-Jensen et al. (2012) for the $\text{Ly}\alpha$ survey and Michałowski et al. (2012) and Perley et al. (2014) for the radio observations.

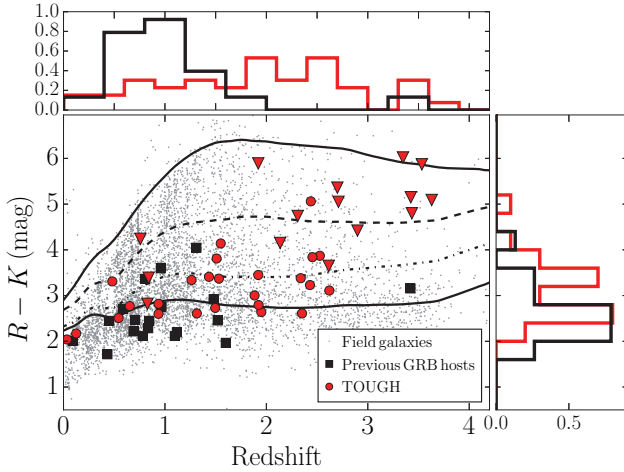


Fig. 4 Redshift dependence of GRB host $R - K$ color. Red data show the TOUGH measurements, where downward triangles denote upper limits (detections in R , upper limits in K). Black data points show literature values (compiled in Savaglio et al. 2009). The background sample are galaxies from the FIREWORKS catalog, and black lines are redshift tracks for different galaxy models (Ell, S0, Sbc and Irr from large or red $R - K$ to blue $R - K$ colors).

3.2 The X-shooter emission line survey

After the high detection rate of GRB hosts in the TOUGH survey, we tried to better physically characterize these systems. Given the long-standing discussion whether the relation between SFR and GRB-rate is a function of metallicity, one of the primary interest was to measure the gas-phase properties for a significant sample of GRB hosts.

Primary tracers of the physical properties of the hot gas at cosmological redshifts are the forbidden transition of oxygen and nitrogen ($[\text{O II}]$, $[\text{O III}]$, $[\text{N II}]$) as well as the most prominent lines of the Balmer series. However, all of these transitions are redshifted into the NIR above $z \sim 1$. As a consequence, most emission-line studies of GRB hosts were previously performed at the lowest redshifts only.

Because of its NIR wavelength coverage and its high efficiency, X-shooter is ideally suited to study GRB host at higher redshift. X-shooter operates in three dichroic-separated arms simultaneously covering the wavelength range between 3000 \AA and 24800 \AA in a single integration. It has a resolving power of around $R \sim 5000$ to $R \sim 10000$ in typically used configurations.

We collected X-shooter spectroscopy for 89 γ -ray-burst-selected galaxies at $0.1 < z < 3.6$ to assemble the most comprehensive emission-line survey of GRB hosts yet available. 75 % of them are at $0.5 < z < 2.5$, with a median redshift $z_{\text{med}} \sim 1.6$, much larger than any previous spectroscopic studies. These data provide systemic redshifts, star-formation rates, visual attenuations, metallicities and velocity dispersions for an unprecedented sample of GRB hosts.

With this survey, we could trace the evolution of GRB-selected galaxies back to $z \sim 3.5$ finding a very strong change of their average physical properties with

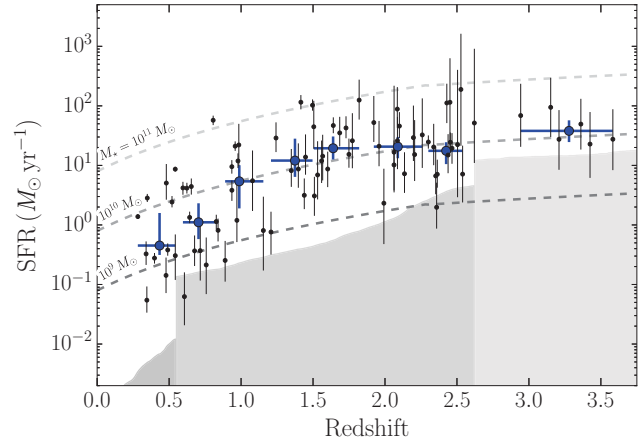


Fig. 5 Dependence of SFR on redshift for GRB hosts. Black data and error bars represent individual galaxies, and blue data the median values binned in redshift with bootstrapped errors. The grey-shaded areas represent our average sensitivity. The three dashed lines show average SFRs for differently massive galaxies derived through the main sequence for a qualitative estimate of the evolution of field galaxies.

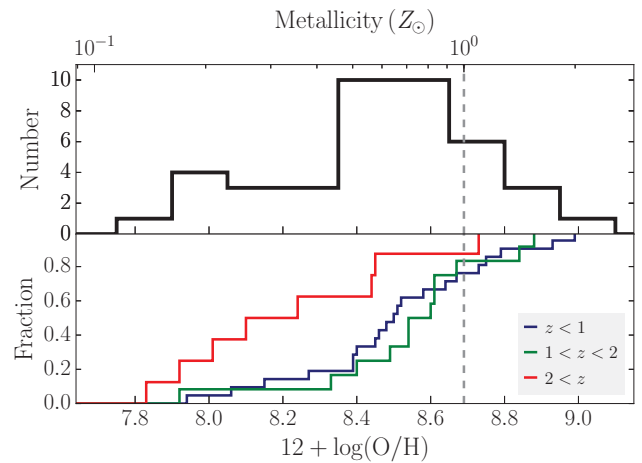


Fig. 6 Histogram (*top panel*) and cumulative, redshift-dependent distribution (*bottom panel*) of gas-phase emission metallicity of GRB-hosting galaxies.

redshift. Below $z \sim 2$, for example, the median SFR of GRB hosts increases from $0.4 M_{\odot} \text{ yr}^{-1}$ at $z \sim 0.4$ up to $\sim 15 M_{\odot} \text{ yr}^{-1}$ at $z \sim 2$ (see Fig. 5). This is qualitatively similar to field-galaxies as indicated by the dashed-lines in Fig. 5.

The metallicities of the galaxies range between 0.1 and 2 times the solar value (Fig. 6). The distribution of metallicities appears very similar at $z < 1$ and $1 < z < 2$, but shifts to lower values at $z > 2$. The fraction of GRB-selected galaxies with super-solar metallicities is $\sim 20\%$ at $z \sim 0.6$. Despite a high abundance of dark GRB hosts in our sample, this fraction is significantly less than the contribution of similarly metal-rich galaxies to the star-formation density at this redshift. It thus confirms a dependence of the GRB rate on metallicity at low-redshift.

At high-redshift ($z \sim 3$), sensitivity limits us to probing only the most luminous GRB hosts for which we measure gas-phase metallicities of $Z < 0.5 Z_{\odot}$. Together with a high incidence of $Z \sim 0.5 Z_{\odot}$ galaxies at $z \sim 1.5$, this shows that the metallicity dependence observed at low redshift will not have a dominant effect at $z \sim 3$.

These properties of GRB hosts and their evolution with redshift can then be understood in a cosmological context of star-forming galaxies together with a picture in which the GRB host properties at low redshift ($z < 1$) are influenced by the GRB's preference to occur in metal-poor environments. At $z \sim 3$, this metallicity effect is expected to be minimal due to the chemical evolution of galaxies, providing evidence that GRB hosts are much more homogeneous probes of star-formation at high redshift.

4 GRB-selected galaxies in absorption

Arguably the most detailed, but certainly most unique information about galaxies with GRBs is obtained in absorption by using the bright afterglow as background light-source. The intervening material is then probed by the GRB's Damped Lyman-alpha (DLA) absorber. A plethora of associated absorption lines from different metal ions in various degrees of ionization and excited states provides unprecedented insights into the chemical composition and physical state of the inter-stellar matter in these high- z galaxies.

4.1 GRB-DLAs at the highest redshift

In particular at the highest redshifts ($z > 5$), where the DLAs towards QSOs become increasingly rare, GRB-DLAs offer a possibility to study in detail typical star-forming galaxies in the early phases of the Universe (Figure 7). Without a GRB as a sign-post, and an afterglow as a lighthouse, similar galaxies would remain beyond reach for even the deepest spectroscopic surveys for years to come.

A number of recent studies performed with X-shooter are noteworthy: The observation of Thöne et al. (2013) of GRB 100219A at $z = 4.7$, a $z = 5.0$ GRB-DLA and an intervening absorber at $z = 4.6$ (Sparre et al. 2014), as well as the spectroscopy of GRB 130606A at $z = 5.9$ by Hartoog et al. (2014).

These data provide the first detailed measurements of metal abundances at $5 < z < 6$, a region in which QSO-DLAs are currently not found. Figure 7 summarized the state-of-the-art for the two DLA families. Conspicuous is the strong trend of declining metallicity with redshift for QSO-DLAs, with an average as low as $[X/H] = -2.3$ at $z \sim 5$. In contrast, GRB-DLAs are, on average, more metal-rich and the evolution of their metallicity with redshift seems to be more subtle.

This is not totally unexpected: the impact parameters, i.e., the differences between the sight-line and the galaxy center, are much smaller for GRB-DLAs than for QSO-DLAs. GRB-DLAs thus probe the central regions of their

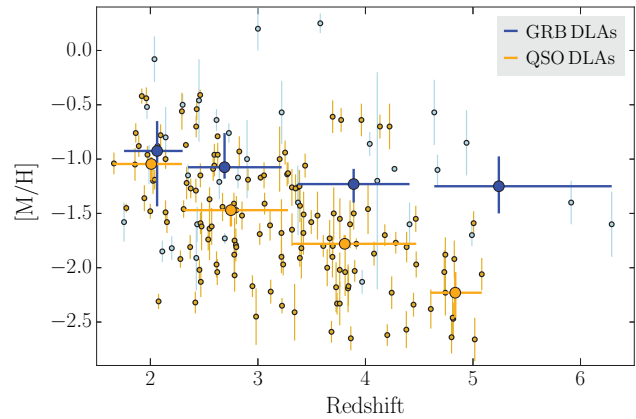


Fig. 7 GRB and QSO-DLA metallicity as a function of redshift. Yellow small/big points are QSO-DLAs and their average values, while blue small/big points represent GRB-DLAs.

hosts, where metallicity enrichment is higher and takes place faster than at the more remote and less dense regions probed by QSO-DLAs.

However, number statistics are still small and more high-quality GRB afterglow spectra are needed to assess the evolution of galaxy metallicity, and the potential differences to QSO-DLAs, up to the highest redshifts.

4.2 GRB-DLAs with molecular gas

The formation of stars is tightly correlated with the presence of molecular hydrogen H_2 , the most abundant molecule in the Universe. Because the absorption signatures of H_2 , the Lyman-Werner bands, are located bluewards of the Lyman α transition, H_2 is probed in detail at $z > 2$ through high-resolution spectroscopy from ground. The presence of H_2 is correlated with the abundance of dust, because dust catalyzes the formation of molecules on its surface and shields against UV photons which otherwise would photodissociate H_2 .

Previously, the best studied GRB-DLAs were those with little dust along their sight-lines. Dust absorbs photons in the near-UV efficiently making high-resolution spectroscopy unfeasible. As a consequence, H_2 remained elusive for a long time along GRB sight-lines.

In the recent years this limitation was overcome, and a number of H_2 bearing GRB-DLAs were discovered (D'Elia et al. 2014; Friis et al. 2014; Prochaska et al. 2009). Out of those, GRB 120815A is one of the most prominent cases (Krühler et al. 2013). However, not only H_2 is studied in GRB afterglow spectra, also rarer molecules like CH^+ have been detected recently (Fynbo et al. 2014).

The properties of the text-book GRB 120815A DLA, such as the metallicity ($[Zn/H] = -1.15 \pm 0.12$), relative abundance ($[Zn/Fe] = 1.01 \pm 0.10$) and visual extinction ($A_V < 0.15$ mag), are relatively common among GRB-DLAs. They are likely typical for the population of GRB-DLAs in general including those that are too faint to study in detail. Figure 8 shows the H_2 -bearing sight-lines of GRB

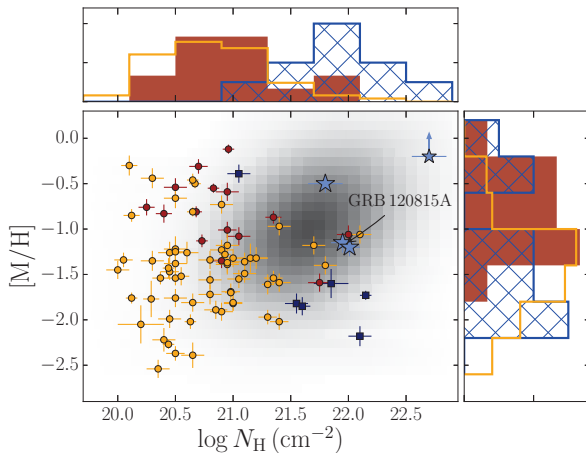


Fig. 8 The central panel shows absorption metallicity vs. N_{H} for QSO and GRB-DLAs. Red and yellow circles correspond to QSO-DLAs with and without significant molecular hydrogen. Blue data are GRB-DLAs and the blue stars are GRBs where H_2 has been detected. The grey background shading indicates the parameter space where many of the more dust-extinguished GRB-DLAs are located. Adapted from Krühler et al. (2013).

and QSO-DLAs as a function of their metallicity $[X/H]$ and neutral hydrogen column density N_{H} .

The shaded area in Fig. 8 illustrates the parameter space in which many more GRB-DLAs are located. GRB-DLAs in this region are, however, usually not studied in high-enough detail, because of their UV-faintness caused by dust attenuation. The detection rate of molecular gas in GRB-DLAs is thus likely to increase further once similar afterglows are observed routinely at higher spectral resolution with the upcoming generation of telescopes and instruments.

5 Summary

Galaxies hosting GRBs provide independent, complementary and very unique information to help understanding star-formation, galaxy evolution and the chemical enrichment of the Universe. We have all the tools at hand right now to exploit these opportunities: A sensitive satellite mission with *Swift*, providing accurate localization and a decent number statistics with 2 triggers per week. A suite of sensitive photometric follow-up instruments that can quickly identify a large fraction of all GRB optical/NIR afterglows. And, last-but-not-least, the newest generation of spectrographs now in operation provides the key data to investigate high-redshift galaxies in an unprecedented way by using GRBs and their bright afterglows.

Acknowledgements. It is a pleasure to thank D. Malesani, J. Fynbo, P. Schady, J. Greiner, J. Hjorth, A. Kann, D. Perley, S. Schulze, for help, inspiring discussions and collaboration over the last years. I also thank very much the Astronomische Gesellschaft, and in particular the organizing team for making this such an inspiring and enjoyable conference.

References

- Cenko, S. B., Kelemen, J., Harrison, F. A., et al. 2009, *ApJ*, 693, 1484
- Covino, S., Melandri, A., Salvaterra, R., et al. 2013, *MNRAS*, 432, 1231
- D’Elia, V., Fynbo, J. P. U., Goldoni, P., et al. 2014, *A&A*, 564, A38
- Friis, M., De Cia, A., Krühler, T., et al. 2014, *MNRAS*, in press, arXiv:1409.6315
- Fynbo, J. P. U., Krühler, T., Leighly, K., et al. 2014, *A&A*, 572, A12
- Fynbo, J. P. U., Starling, R. L. C., Ledoux, C., et al. 2006, *A&A*, 451, L47
- Gehrels, N., Chincarini, G., Giommi, P., et al. 2004, *ApJ*, 611, 1005
- Greiner, J., et al. 2008, *PASP*, 120, 405
- Greiner, J., Krühler, T., Fynbo, J. P. U., et al. 2009, *ApJ*, 693, 1610
- Greiner, J., Krühler, T., Klose, S., et al. 2011, *A&A*, 526, A30
- Hartoog, O. E., Malesani, D., Fynbo, J. P. U., et al. 2014, *A&A*, submitted, arXiv:1409.4804
- Hjorth, J., Malesani, D., Jakobsson, P., et al. 2012, *ApJ*, 756, 187
- Hjorth, J., Sollerman, J., Møller, P., et al. 2003, *Nature*, 423, 847
- Jakobsson, P., Hjorth, J., Malesani, D., et al. 2012, *ApJ*, 752, 62
- Kistler, M. D., Yüksel, H., Beacom, J. F., Hopkins, A. M., & Wyithe, J. S. B. 2009, *ApJ*, 705, L104
- Krühler, T., Greiner, J., Schady, P., et al. 2011a, *A&A*, 534, A108
- Krühler, T., Küpcü Yoldaş, A., Greiner, J., et al. 2008, *ApJ*, 685, 376
- Krühler, T., Ledoux, C., Fynbo, J. P. U., et al. 2013, *A&A*, 557, A18
- Krühler, T., Malesani, D., Milvang-Jensen, B., et al. 2012, *ApJ*, 758, 46
- Krühler, T., Schady, P., Greiner, J., et al. 2011b, *A&A*, 526, A153
- Kumar, P., & Zhang, B. 2014, *Phys. Rep.*, in press, arXiv:1410.0679
- Michałowski, M. J., Kamble, A., Hjorth, J., et al. 2012, *ApJ*, 755, 85
- Milvang-Jensen, B., Fynbo, J. P. U., Malesani, D., et al. 2012, *ApJ*, 756, 25
- Perley, D. A., Cenko, S. B., Bloom, J. S., et al. 2009, *AJ*, 138, 1690
- Perley, D. A., Levan, A. J., Tanvir, N. R., et al. 2013, *ApJ*, 778, 128
- Perley, D. A., Perley, R. A., Hjorth, J., et al. 2014, *ApJ*, in press, arXiv:1407.4456
- Pian, E., Mazzali, P. A., Masetti, N., et al. 2006, *Nature*, 442, 1011
- Prochaska, J. X., Sheffer, Y., Perley, D. A., et al. 2009, *ApJ*, 691, L27
- Robertson, B. E., & Ellis, R. S. 2012, *ApJ*, 744, 95
- Rossi, A., Klose, S., Ferrero, P., et al. 2012, *A&A*, 545, A77
- Savaglio, S., Glazebrook, K., & Le Borgne, D. 2009, *ApJ*, 691, 182
- Sparre, M., Hartoog, O. E., Krühler, T., et al. 2014, *ApJ*, 785, 150
- Tanvir, N. R., Fox, D. B., Levan, A. J., et al. 2009, *Nature*, 461, 1254
- Tanvir, N. R., Levan, A. J., Fruchter, A. S., et al. 2012, *ApJ*, 754, 46
- Thöne, C. C., Fynbo, J. P. U., Goldoni, P., et al. 2013, *MNRAS*, 428, 3590
- Vreeswijk, P. M., Fruchter, A., Kaper, L., et al. 2001, *ApJ*, 546, 672